European Conference on Optical Communication (ECOC) 2022 © Optica Publishing Group 2022

Wafer-scale fabrication of low-loss waveguides in lithium niobate on insulator (LNOI) integrated photonics platform

Jacopo Leo*, Mozhgan Hayati, Farnaz Ebrahimi Agri, Zyad Haddad, Gregory Choong, Yves Petremand, Ivan Prieto, Olivier Dubochet, Michel Despont, Hamed Sattari, Amir Ghadimi*

Swiss Center for Electronics and Microtechnology (CSEM),
Corresponding authors: *jacopo.leo@csem.ch, *amir.ghadimi@csem.ch

Abstract *Here, we present a wafer scale fabrication for low-loss lithium niobate on insulator (LNOI) waveguides at C-band and statistical measurements of resonators, demonstrating quality factors exceeding* 2.5×10^6*, corresponding to a waveguide loss below 0.14 dB/cm. ©2022 The Author(s)*

Introduction

Lithium niobate (LiNb) is one of the most promising photonics materials that comprises a unique set of interesting optical properties[1],[2] such as: a high electro-optic (EO) coefficient, high intrinsic 2^{nd} and 3^{rd} order nonlinearities, and a large transparency window (350 nm - 5500 nm). Recent advancements in bonding of single crystal thin films LiNb onto silicon substrates[3], also known as lithium niobate on insulator (LNOI), opens a new avenue to explore the advantages of LiNb in the context of photonics integrated circuits (PICs)[4],[5] that promises for further miniaturization, cost reduction, salable manufacturing and integration. In the LNOI platform, waveguides are fabricated using reactive ion etching (RIE) in an LNOI thin film. This allows for the reduction of mode volumes by more than 100x[6] in comparison with the conventional waveguides in bulk LiNb, which not only results in more efficient and faster modulators[7] but also in significantly smaller bending radii and PIC footprints . This ultimately enables designing complex PICs with tens of components in a millimeters-size chips[8].

In the past few years, there has been a tremendous progress in demonstrating various electro-optics and nonlinear optical effects in LNOI in key milestones experiments such as high speed, low V_π electro-optical modulators[7], Kerr and EO optical frequency combs[9],[10], wavelength conversion[11], supercontinuum generation[12] and self-referencing[13],[14]. These impressive results so far, have been limited to few academic groups around the world. Thus, establishing a reliable, high quality and high-yield ”foundry like” fabrication process[15] for LNOI PICs is the key to ensure that these academic progresses translates into an industrial scale technology and makes the LNOI photonics an accessible platform to a wide range of photonics designers and end-users. CSEM is set to establish an LNOI PIC foundry based on a well-tested process design kit (PDK) library. To reach this goal we have established a full PIC development chain encompassing design, simulation, layouting, fabrication, and characterization steps.

One major milestone towards a reliable LNOI PIC platform is to realize low loss waveguides[5],[16], crucial to on-chip routing and enabling high performance passive and active components. Here, we present our results toward this goal and demonstrate a wafer-scale fabrication technology for low-loss LNOI waveguides at telecommunication C-band.

Technology and Fabrication

The technology cross-section along with few SEM images of the manufactured components in our LNOI PIC platform are shown in Fig. 1.

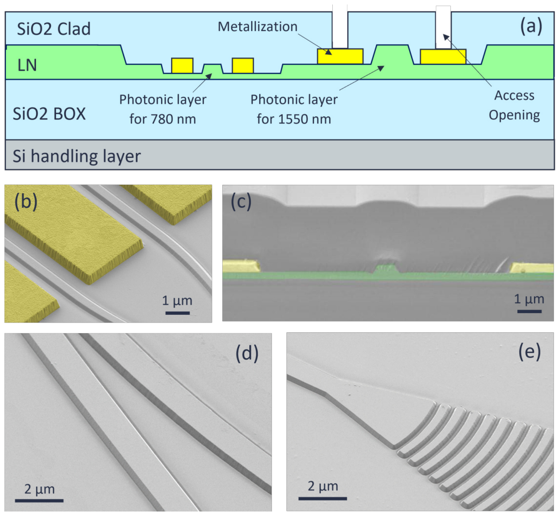

Fig. 1 a) CSEM's LNOI PIC platform technology cross-section. SEM images of b) an electro-optical modulator at 780 nm (colored), c) the cross-section showing the LN waveguide with the electrodes forming a phase shifter (colored), d) coupled waveguides, and e) a grating coupler.

The waveguide fabrication technology is based on commercially available LNOI 6-inch wafers (from NanoLN co.). The LNOI stack consists of a 600 nm thick single crystal x-cut LiNb layer on top

European Conference on Optical Communication (ECOC) 2022 © Optica Publishing Group 2022

of a 4.7 μm buried thermal oxide (BOX) layer (see Fig. 1). The device layer hosts two types of rib waveguides defined by their ridge height. A 600 nm high waveguide serving for the wavelength window of short wavelength infrared (SWIR) of around 1550 nm and a 200 nm high waveguide devised for near infrared (NIR) and visible spectrum. For the 1550 nm layer, the PICs are patterned in hydrogen silsesquioxane (HSQ) using electron beam lithography (EBL) and are etched 400 nm into LiNb layer using an Ar^+ ion milling technology. We then use the remaining 200 nm LiNb layer for 780 nm PIC layer, which are also patterned by EBL and etched 150 nm using Ar^+ ion milling. The device layer waveguide processing ensures smooth side walls (see Fig.1) that is crucial for a low propagation loss. The next steps consist of metallization of electrodes for active components using a 500 nm gold liftoff process and deposition of 3 μm of SiO2 cladding to protect the PIC from environmental damages and create a symmetric index contrast in top and bottom of the waveguides. The cladding can be locally removed to create electrical access to electrodes and allows for claddless waveguides and resonators if needed (e.g. for dispersion engineering[17]).Thanks to a final chip release process which is done by a deep etching into the Si substrate we manufacture LNOI PICs in various sizes and are not limited to a staircase dicing pattern. The fully processed chips hosting a variety of passive and active components are shown in Fig. 2.

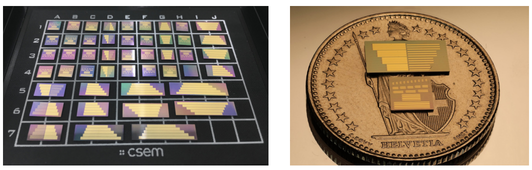

Fig. 2 LNOI chips of various size fabricated by CSEM

Characterization

To characterize the propagation loss in the platform an extensive measurement campaign is required to obtain a loss statistics, which is elusive by measuring only a few number of waveguides. To be able to measure the waveguide losses independently and discard the effect of the fiber to chip coupling loss, we measured a set of racetrack resonators. The layout of the measured chip is shown within Fig. 3 which encompasses a sweep of racetrack micro-ring resonators with identical bending radius but varying the straight section lengths. The resonator and bus waveguide width are fixed to 1500 nm and 800 nm, respectively. In such a configuration, the linewidth/quality factor of the resonator will reflect the total loss in the micro-ring resonator. By extracting the trend in the intrinsic quality factor of the series of the resonator, we can deduce the propagation loss of the straight waveguide section. Furthermore, the statistic which is obtained through thousands of resonances measurement from dozens of resonators of different geometries provides us with information about our process repeatability and the geometry variation, helping us to understand the different sources of propagation losses in our LNOI PIC platform.

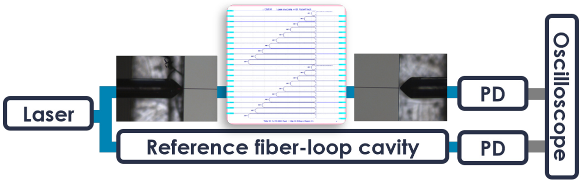

Fig. 3 Measurement setup to characterize LiNb resonator chip with laser, fiber lens, photo-diode (PD) and oscilloscope

A schematic of our setup is shown in Fig. 3. A mode hop free tunable laser light with an emission range from 1510 nm to 1630 nm is splitted into two different paths. The first path is sent to the LNOI chip through a Polarization Controller (PC) to select either horizontal or vertical polarizations and the second path to a reference fiber-loop cavity. The fiber-chip coupling is realized by lensed fibers from the edge of the chip, and are mounted on an XYZ stage. The initial alignment on the first waveguide is manually adjusted. To increase the coupling, a fine tuning is computed remotely by a XYZ stage's piezo motor. For following racetrack measurement, the chip is settled onto a piezo linear actuator, which is automatically driven to align the subsequent waveguide. At the end of the two optical paths, the transmission and reference are evaluated by two fast photodetectors. Finally, the photodetectors responses are acquired using a 500 MHZ bandwidth oscilloscope.

Measurement Result

To identify the propagation loss in the LNOI waveguides, we have measured the optical transmission of LNOI racetrack resonators from wavelengths going from 1510 nm to 1630 nm. Two racetracks transmission responses with different straight lengths are shown in Fig. 4(a). For each resonance, the propagation loss is evaluated via intrinsic linewidth $\kappa_0/2\pi$. To identify κ_0 a lorentzian is fitted on the resonance response (Fig. 4(b)), and its fitting parameters are extracted (Full Width Half Maximum Δf_{FWHM} and the Extinction Ratio ER). $k_0/2\pi$ is then calculated from the following equation (using the assumption of under coupled resonator which estimates a higher value for $k_0/2\pi$)[18].

$$\kappa_0 = \Delta f_{FWHM} \pi (1 + \sqrt{\mathrm{ER}}) \qquad (1)$$

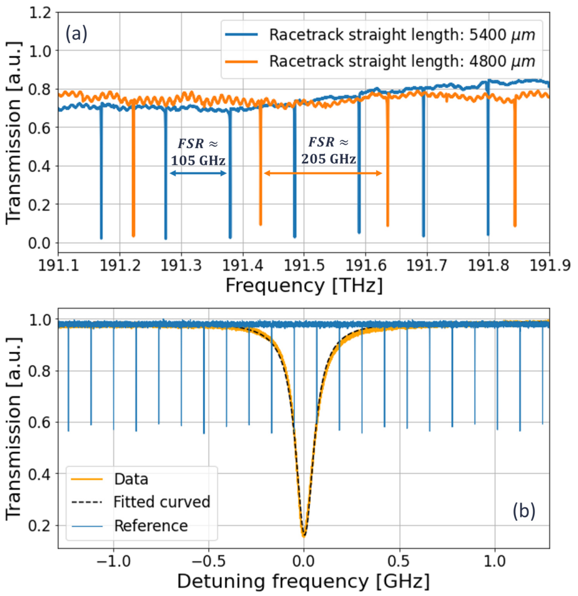

Fig. 4 (a) LNOI racetrack resonator's transmission for different straight length illustrating the scaling of FSR with resonator's length (b) LNOI racetrack transmission (orange) with lorentzian fitting (dashed black) and fiber-loop referenced resonator (blue) with calibrated FSR=118 MHz

Finally, to calculate the linear propagation losses of LNOI waveguide, we used the measured $k_0/2\pi$ and the simulated effective refractive index $n_{eff} \approx 1.94$ via finite element method (Eq. 2):

$$loss\ [\mathrm{dB/m}] = -10 \cdot \log_{10}(e) \kappa_0 \frac{n_{eff}}{c} \qquad (2)$$

Discussion

The histograms of intrinsic linewidth in Fig. 5(a) and plot of intrinsic quality factor versus resonator's straight length in Fig. 5(b) show a clear trend in which lower linewidth ($\equiv$ higher Qs) is achieved in racetracks with longer straight section. This can be a strong indication that the quality factor of our current devices is limited by the bending losses at the two ends of the racetrack resonator[5] rather than the propagation losses of the straight waveguides. We use bending radii of 100 $\mu\mathrm{m}$ for this series of racetracks. We obtain quality factor of only $\approx 0.6 \times 10^6$ (pick histograms in Fig. 5(b)) for a circular ring resonator with 100 $\mu\mathrm{m}$ radius which is merely limited due to the bending loss, while for the longest racetrack (straight length = 4.8 mm) we obtain a high quality factor of 2.5×10^6. Such linear upward trend is explained by that fact that the contribution of the bending losses at two ends is getting proportionally smaller in larger resonators. Even with these bending loss limited measurements, we estimate linear propagation losses below < 0.14 dB/cm which is an upper limit for our LNOI waveguides.

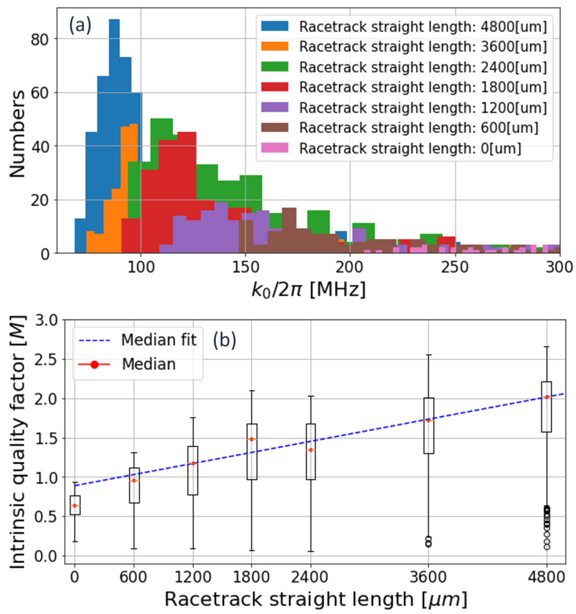

Fig. 5 (a) Histograms of intrinsic linewidth versus resonator's straight length (b) Boxplots of intrinsic quality factor versus resonator's straight length

Conclusions

We presented our recent results towards enabling a low loss wafer scale LNOI PIC platform. Thanks to a reliable LNOI waveguide etching process we have statistically measured waveguides with an intrinsic quality factor greater than 2.5×10^6, corresponding to a linear waveguide loss below 0.14 dB/cm. This promises for large scale monolithic LNOI photonics with a wide range of different applications. Our results and analysis show that we are still limited to the bending loss in the specific structures we measure, and the straight waveguide propagation loss are estimated to be even lower than the numbers reported here. Although we are further improving our processing to obtain even lower propagation losses, these results are already in the ballpark of mature PIC platforms and promise for a low loss monolithic LNOI PIC platform that can be offered as a reliable foundry service to the PIC community.

Acknowledgements

This project has received funding from the European Union's Horizon 2020 (grant agreement N° 101016138) and Swiss National Science Foundation (SNSF) (194693)

European Conference on Optical Communication (ECOC) 2022 © Optica Publishing Group 2022

References

[1] D. Zhu, L. Shao, M. Yu, *et al.*, "Integrated photonics on thin-film lithium niobate", *Advances in Optics and Photonics*, vol. 13, Jun. 2021. DOI: 10.1364/AOP.411024.

[2] D. Nikogosyan, "Nonlinear optical crystals: A complete survey", *Nonlinear Optical Crystals: A Complete Survey: , ISBN 978-0-387-22022-2. Springer Science+Business Media, Inc., 2005*, Jan. 2005. DOI: 10.1007/b138685.

[3] P. Rabiei and P. Gunter, "Optical and electro-optical properties of submicrometer lithium niobate slab waveguides prepared by crystal ion slicing and wafer bonding", *Applied Physics Letters - APPL PHYS LETT*, vol. 85, Nov. 2004. DOI: 10.1063/1.1819527.

[4] C. Wang, M. Burek, Z. Lin, *et al.*, "Integrated high quality factor lithium niobate microdisk resonators", *Optics Express*, vol. 22, pp. 30 924–30 933, Dec. 2014. DOI: 10.1364/OE.22.030924.

[5] M. Zhang, C. Wang, R. Cheng, A. Shams-Ansari, and M. Loncar, "Monolithic ultrahigh-q lithium niobate microring resonator", *Optica*, vol. 4, Dec. 2017. DOI: 10.1364/OPTICA.4.001536.

[6] C. Wang, M. Zhang, B. Stern, M. Lipson, and M. Loncar, "Nanophotonic lithium niobate electro-optic modulators", *Optics Express*, vol. 26, Jan. 2017. DOI: 10.1364/OE.26.001547.

[7] C. Wang, M. Zhang, X. Chen, *et al.*, "Integrated lithium niobate electro-optic modulators operating at cmos-compatible voltages", *Nature*, vol. 562, Oct. 2018. DOI: 10.1038/s41586-018-0551-y.

[8] Y. Qi and Y. Li, "Integrated lithium niobate photonics", *Nanophotonics*, vol. 9, Apr. 2020. DOI: 10.1515/nanoph-2020-0013.

[9] M. Zhang, B. Buscaino, C. Wang, *et al.*, "Broadband electro-optic frequency comb generation in a lithium niobate microring resonator", *Nature*, vol. 568, Apr. 2019. DOI: 10.1038/s41586-019-1008-7.

[10] Z. Gong, X. Liu, Y. Xu, *et al.*, "Soliton microcomb generation at 2 î¼m in z-cut lithium niobate microring resonators", *Optics Letters*, vol. 44, p. 3182, Jun. 2019. DOI: 10.1364/OL.44.003182.

[11] C. Wang, X. Xiong, N. Andrade, *et al.*, "Second harmonic generation in nano-structured thin-film lithium niobate waveguides", *Optics Express*, vol. 25, Oct. 2016. DOI: 10.1364/OE.25.006963.

[12] M. Yu, B. Desiatov, Y. Okawachi, A. Gaeta, and M. Loncar, "Coherent two-octave-spanning supercontinuum generation in lithium-niobate waveguides", *Optics Letters*, vol. 44, p. 1222, Mar. 2019. DOI: 10.1364/OL.44.001222.

[13] E. Obrzud, S. Denis, H. Sattari, *et al.*, "Stable and compact rf-to-optical link using lithium niobate on insulator waveguides", *APL Photonics*, vol. 6, p. 121 303, Dec. 2021. DOI: 10.1063/5.0070103.

[14] Y. Okawachi, M. Yu, B. Desiatov, *et al.*, "On-chip self-referencing using integrated lithium niobate waveguides", *Optica*, vol. 7, May 2020. DOI: 10.1364/OPTICA.392363.

[15] E. Agrell, M. Karlsson, A. Chraplyvy, *et al.*, "Roadmap on optical communications", *Journal of Optics*, vol. 18, May 2016. DOI: 10.1088/2040-8978/18/6/063002.

[16] A. Shams-Ansari, G. Huang, L. He, *et al.*, "Reduced material loss in thin-film lithium niobate waveguides", *arXiv preprint arXiv:2203.17133*, 2022.

[17] C. Wang, C. Langrock, A. Marandi, *et al.*, "Ultrahigh-efficiency wavelength conversion in nanophotonic periodically poled lithium niobate waveguides", *Optica*, vol. 5, p. 1438, Nov. 2018. DOI: 10.1364/OPTICA.5.001438.

[18] H. A. Haus, *Waves and Fields in Optoelectronics (Prentice-Hall series in solid state physical electronics)*. Englewood Cliffs, NJ: Prentice Hall, Inc., 1983. DOI: 10.1088/0031-9112/35/8/023.